J Mater Sci (2015) 50:1666–1672
DOI 10.1007/s10853-014-8727-9

Synthesis of ultra-small silicon nanoparticles by femtosecond laser ablation of porous silicon

V. S. Vendamani · Syed Hamad · V. Saikiran · A. P. Pathak · S. Venugopal Rao · V. V. Ravi Kanth Kumar · S. V. S. Nageswara Rao

Received: 30 July 2014 / Accepted: 15 November 2014 / Published online: 2 December 2014

Abstract We report a detailed study on the synthesis of ultra-small (1–10 nm) colloidal silicon nanoparticles (Si NPs) by ablating porous silicon (pSi) in acetone using femtosecond laser pulses. Porous silicon is considered as a target material for ablation because it contains a large number of light emitting silicon nanoparticles. The pSi samples were prepared by anodic etching of silicon in aqueous HF solution for different etching current densities. Transmission electron microscope measurements confirmed the successful formation of well-isolated spherical silicon nanoparticles. The average size of spherical NPs were estimated to be ~7.6, ~7, and ~6 nm when anodic etching current densities of 5, 10, and 20 mA/cm^2 were used respectively for preparing pSi targets. The crystallinity of these Si NPs was confirmed by selective area electron diffraction and Raman spectroscopy measurements. The observed blue shift in the absorption and emission spectra are attributed to reduction in the average particle size with increase in etching current density. These Si NPs may be useful for fabricating low-dimensional microelectronic compatible photonic devices.

V. S. Vendamani · S. Hamad · V. Saikiran · A. P. Pathak · S. V. S. Nageswara Rao (✉)
School of Physics, University of Hyderabad, Hyderabad 500046, India
e-mail: nageshphysics@gmail.com; svnsp@uohyd.ernet.in

V. S. Vendamani · V. V. Ravi Kanth Kumar
Department of Physics, Pondicherry University, Puducherry 605014, India

S. Venugopal Rao
Advanced Center of Research in High Energy Materials (ACRHEM), University of Hyderabad, Hyderabad 500046, India

Introduction

Silicon nanoparticles (Si NPs) are promising candidates for building block materials in the fields of nanotechnology and nanophotonics [1–6]. In the present scenario, a challenging task is to prepare impurity-free, ultra-small, and high density silicon nanoparticles in short duration. The size-tunable optical and electronic properties of Si NPs make them potential candidates for use in light emitting diodes (LED), quantum dot lasers, chemical sensors, printed electronics, floating gates, and flexible solar cells [7–11]. Furthermore, ultra-small Si NPs have relevance in photovoltaics owing to their enhanced absorption in UV region. Si NPs with diameters in the range of 1–3 nm are used as red–green–blue (RGB) emitters in optoelectronic devices [12, 13]. There are copious reports on the production of size-controlled Si NPs by various techniques such as electrochemical etching [2, 3, 14], ion-implantation of Si into SiO_2 matrix followed by annealing processes [15, 16], chemical vapor deposition (CVD) [17], and laser ablation [18, 19]. Although the Si NPs produced by different procedures appear to be identical, their optical responses can differ drastically. Hence, it is important to understand various mechanisms that are useful for preparing ultra-small silicon nanoparticles.

Laser ablation in liquids is a versatile method to synthesize size-controlled colloidal Si NPs. This technique facilitates the fabrication of well-dispersed, impurity-free, and size-tunable nanoparticles in a short duration. There are many laser parameters such as laser wavelength, energy per pulse, pulse duration, focal spot area, repetition rate, and liquid medium [20], which can control the size, shape, and density of nanoparticles. Particularly, the laser pulse duration is found to affect directly the ablation, nucleation, growth, and aggregation mechanisms [21–24]. Especially,

laser ablation by ultra-short laser pulses has been an attractive technique to synthesize isolated nanoparticles, as compared to ablation by nanosecond (ns) pulses because there is a little or no collateral damage due to shock waves and heat conduction produced in the material. Long laser pulses (ns) release their energy slowly to target electrons on the time scales comparable to that of thermal relaxation processes of the target. Femtosecond (fs) laser pulses transfer their energy to target electrons much faster as compared to the time scales of electron–phonon thermalization. Hence the material undergoes ultrafast non-thermal heating and becomes a superheated fluid [25] and an extreme thermo-elastic pressure built in the material are responsible for the generation of nanoparticles in liquid medium. The detailed mechanism of nanoparticle generation under fs laser ablation has been discussed in our previous reports [19, 26, 27].

There are a few earlier reports on the generation of Si NPs by femtosecond (ultra-short pulse) laser ablation under liquid environment [28–31]. Recently Semaltianos, et al. [32] have generated isolated Si NPs by using UV fs pulses. However, it is difficult to achieve smaller nanoparticles (<10 nm) by ablating bulk silicon (generally the size is limited to ~30 nm) [19, 33]. There are few reports available on the synthesis of ultra-small (~1–10 nm) Si nanoparticles by two-stage process using pulsed laser ablation. Recently, Alkis and co-workers [34] have reported the formation of blue luminescent colloidal silicon nanocrystals by two-stage process. They observed reduced particle size ranging between 1 and 5.5 nm with fs laser ablation of Si wafers followed by exposure to ultrasonic waves and by filtering chemical-free post-treatment. Introduction of nanostructured porous silicon (pSi) for ablation could be a very effective and potential method to generate ultra-small silicon nanoparticles for low-dimensional photonic applications.

Here we report a novel method for preparing ultra-small silicon nanoparticles. An attempt has been made to prepare nanoparticles by ablating porous silicon considering the fact that it contains a network of ultra-small light emitting Si NPs. Moreover, the use of pSi as a target material possesses substantially lower thermal conductivity than crystalline Si. Furthermore, use of pSi targets offers additional parameters for controlling the size and shape of nanoparticles by ablation. Some examples of these additional controlling parameters are Si-doping (type and concentration), type of electrolyte and its concentration, etching current density, and etching time, etc. To our knowledge, there are no reports available on the ablation of porous silicon in past. The present study shows that, pSi is a suitable candidate for fabricating ultra-small Si NPs by fs laser ablation. The study also indicates that the ablation of pSi is distinctly different from that of bulk silicon.

Experimental details

Ultra-small Si NPs were synthesized by subjecting the porous silicon targets to fs laser pulses under liquid environment. Porous silicon was prepared by electrochemical (anodic) etching of mirror-polished p-type boron-doped (1–30 Ω cm), single crystal Si (100) wafers which were cut into 1×1 cm^2 pieces and cleaned ultrasonically by acetone for 10 min to remove chemical contaminations. These Si samples were then cleaned with 10 % hydrofluoric (HF) acid to etch the native oxide layer. Then the samples were anodically etched for 10 min in 1:2::HF:Isopropyl alcohol (IPA) solution at different etching current densities $J = 5$, 10, and 20 mA/cm^2. Immediately after the anodization, the samples were rinsed with ethyl alcohol and subsequently with pentane to control the capillary actions. Finally the samples were rinsed in deionized water and left for natural drying. The formation of sponge-like nanostructured pSi has been confirmed by field emission scanning electron microscope (FESEM-Carl ZEISS, FEG, Ultra 55—using 5 keV electrons) and by observing intense visible (near red) luminescence under UV lamp [2]. Two sets of pSi samples were prepared under same conditions. One set was used for the proposed laser ablation work whereas the other set was used as control samples. These control samples were used to estimate the thickness and porosity of pSi layers as a function of etching current density by employing cross-sectional FESEM and gravimetric analysis [14], respectively.

The ultrafast laser source used in this study is a chirped pulse amplified Ti:sapphire laser system (Coherent Legend, ~2.5 W, 1 kHz) delivering nearly bandwidth-limited laser pulses (Pulse duration of ~40 fs) at 800 nm. The pSi target was placed in a Pyrex cell and filled with acetone which was 5 mm above the target surface. Acetone is known to control the growth and aggregation of nanoparticles in much better way due to its high polarity and dipole moment, when compared to other liquids like water and ethanol [35]. This study suggests that acetone is an appropriate medium for ablation of Si-based targets. Hence, acetone was chosen as a medium for this ablation work. The theoretical beam waist estimated at focus on the sample surface was ~30 μm. The targets were placed normal to laser beam on a motorized X–Y stage which was controlled by an ESP 300 motion controller. Target was scanned to avoid multiple ablations from same spot so that every pulse sees a fresh spot on the pSi surface. Therefore the majority of the Si NPs generated by laser ablation are expected to be from the pSi layer. Pulse energies of ~100 μJ were used for ablation which was carried out for ~40 min. The observed change in the color of the acetone (to light-orange) during ablation indicates the formation of Si NPs. The samples were prepared for further

characterization by drop-casting the colloidal Si NPs onto corresponding plates (Cu-coated TEM grid for TEM, Glass cover slips for Raman and PL measurements) and allowing them to evaporate the solution. The formation of Si NPs was confirmed by micro-Raman spectroscopy (WITech Alpha 300 spectrometer–Excitation wavelength: 532 nm Nd-YAG laser, 40 mW, and a grating of 600 lines/mm). Low laser power (5 mW) was used throughout the measurements to avoid local heating effects. The size distribution has been estimated by using Transmission Electron Microscopy (TEM- Technai, equipped with a thermo-ionic electron gun working at 200 kV) measurements. The energy dispersive X-ray spectroscopy (EDS-SEI Technai G2 S-T win 200 keV energy of electron) measurements were also performed to study the chemical contaminations (if any) present in the sample.

High-resolution transmission electron microscopy together with Raman spectroscopy confirmed the generation of Si NPs. Crystalline nature and growth direction of Si NPs were obtained by selective area electron diffraction (SAED). Absorbance (UV–Vis, Jasco V-670) and photoluminescence (PL-Fluorolog, Xenon lamp, 450 W, Exc: 350 nm, resolution: 0.3 nm) measurements were also performed to elucidate the optical behavior of Si NPs.

Results and discussion

FESEM image shown in Fig. 1, confirms the formation of nanostructured porous silicon as a result of electrochemical etching of silicon. The width of pore walls and the size of nanoparticles embedded between the pores decrease with increase in applied current density during electrochemical etching [1, 2]. The refractive index of the pSi layer mainly depends on the size and density of the pores as per the effective medium model. The refractive index of pSi is expected to be lower than that of bulk Si because pSi is effectively a combination of air (in pores) and silicon. [2]. The refractive index of the material is known to influence the ablation process by multi-photon ionization [36]. The thickness and porosity of pSi layers prepared at different etching current densities are presented in the Table 1. Further, the anodized (pSi) samples have been subjected to fs laser pulses to synthesize ultra-small colloidal Si NPs in acetone. TEM images shown in Fig. 2 confirm the formation of nearly spherical Si NPs by laser ablation. From these images, we concluded that the ablation of pSi target prepared at higher current density ($J = 20$ mA/cm^2) produced smaller particles. To determine the accurate size distribution of Si NPs, we have estimated the sizes of more than 500 particles in different regions of TEM grids. The corresponding histograms suggest that the size of Si NPs was in the range of 1–30 nm. Further, it was found that the major portion of the nanoparticles have diameters in the range of 1–10 nm. The size distribution shown in Fig. 2 has been analyzed by performing Gaussian peak fitting to estimate the average particle size (i.e., the center of the Gaussion) presented in Table 2. Laser ablation of pSi targets prepared with current densities of 5, 10, and 20 mA/cm^2 produced Si NPs of average size $\sim$7.6, $\sim$7, and $\sim$6 nm, respectively. EDS measurements were performed to identify the elements that are present in the samples and the data are shown in Fig. 3. The observed peaks related to carbon (C) and copper (Cu) are associated with TEM grids used in this study. Therefore, the main constituent of these samples was found to be Si, as expected. There are no detectable impurities other than a small concentration of oxygen, present in these samples. Hence, these EDS measurements confirm the successful generation of impurity-free ultra-small Si NPs by laser ablation of porous silicon in acetone. The selective area electron diffraction pattern, shown in Fig. 4 reveals the face centered cubic (fcc) structure of Si nanoparticles with a zone axis [111]. HRTEM image (Fig. 4) of a single isolated Si NP shows the crystalline lattice fringes with lattice spacing of

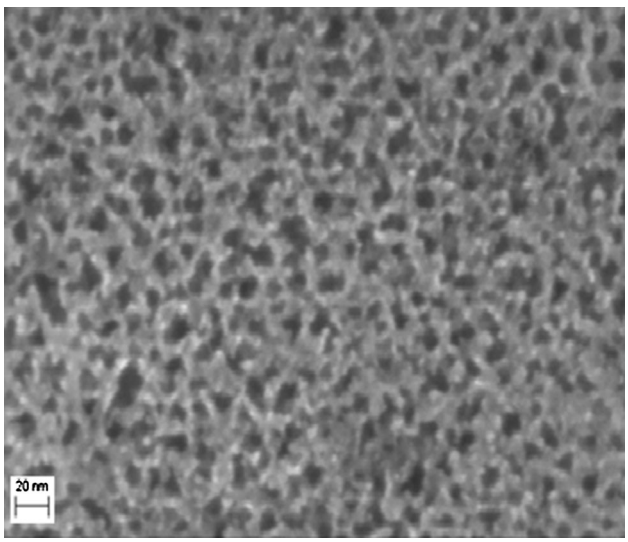

Fig. 1 FESEM image of nanostructured porous silicon (pSi) prepared at current density $J = 10$ (mA/cm^2) by electrochemical etching of Si

Table 1 Physical and optical parameters of pSi used for laser ablation

PSi target used for ablation	Estimated thickness of pSi layer (μm)	Porosity of pSi layer (%)	PL peak position (nm)
pSi-5 mA/cm^2	1.89 ± 0.29	71	651
pSi-10 mA/cm^2	2.31 ± 0.41	76	642
pSi-20 mA/cm^2	3.27 ± 0.25	82	637

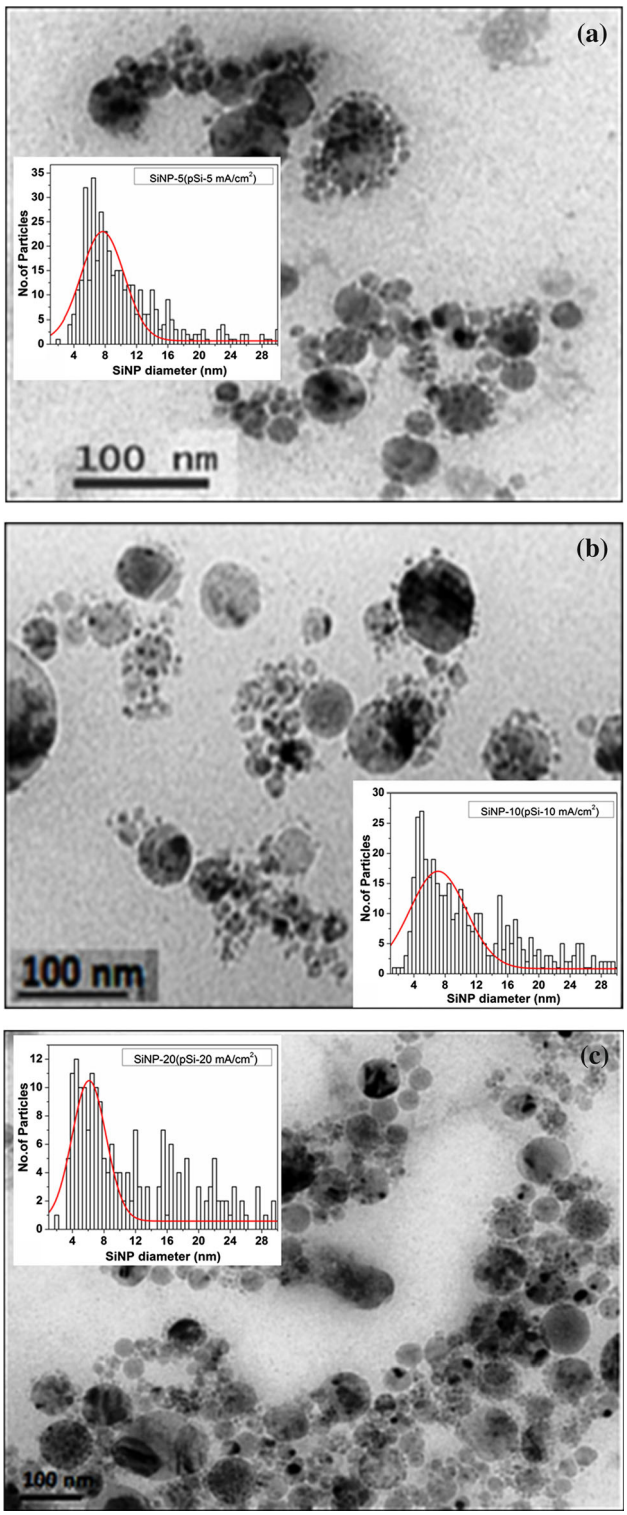

Fig. 2 TEM images and corresponding histograms (*inset*) of Si NPs obtained by femtosecond laser ablation of pSi targets prepared at different etching current densities. **a** pSi-5 mA/cm^2, **b** pSi-10 mA/cm^2, and **c** pSi-20 mA/cm^2 (The *solid lines* in the *insets* represent Gaussian fits of corresponding size distribution)

Table 2 Particle sizes (average diameters) and optical parameters of Si NPs estimated by different analytical techniques

Sample label	PL peak position (nm)	Estimated average particle diameters d (nm)		
		By TEM	By Raman	By UV–Vis
Si NP-5	431	7.6 ± 3.0	5	9
Si NP-10	428	7.0 ± 3.1	3	8
Si NP-15	426	6.1 ± 2.5	2	6

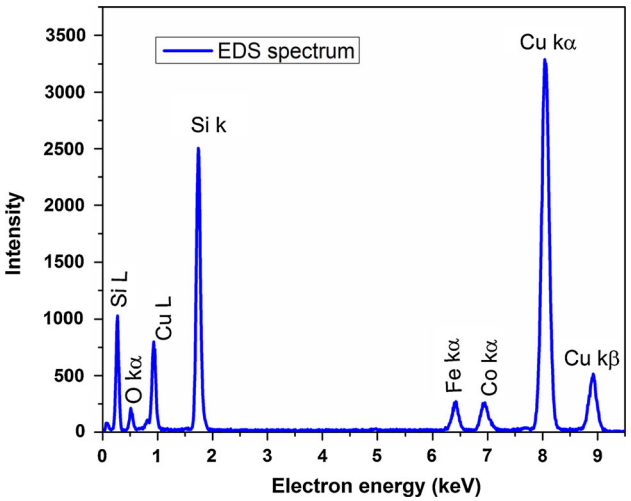

Fig. 3 Energy dispersive X-ray spectrum of Si NPs

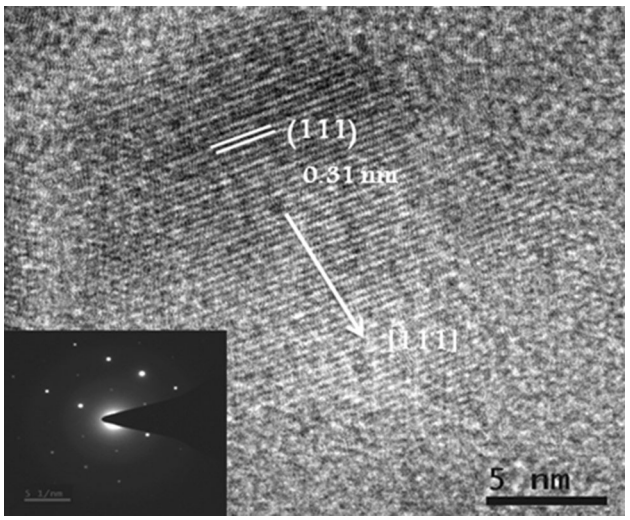

Fig. 4 HRTEM image of a single Si NP, showing the [111] plane and their corresponding electron diffraction pattern (*inset*)

0.31 nm corresponding to the inter-planar spacing of Si [111] plane. The fast Fourier transform (FFT) creates the diffraction pattern of the image in the back focal plane and the corresponding inverse FFT was also constructed by FFT as shown in Fig. 5. These measurements further confirm the fact that the observed nanoparticles are actually made of Si.

The absorption properties of Si NPs have been significant in estimating the optical energy band gaps. The absorption spectra shown in Fig. 6 depict a broad and continuous band between 200 and 500 nm with a distinct peak at around 325 nm. When the ablation was performed on pSi target prepared at higher current densities, a blue shift was observed in the absorption peak position. The shift in the absorption peak position may be attributed to change in the average size of nanoparticles present in the solution.

The Raman spectra of Si NPs generated by fs laser ablation of different pSi targets under acetone environment have also been investigated by using micro-Raman measurements and the data are presented in Fig. 7. Raman spectrum shows a sharp optical phonon band near 520 cm^{-1} with asymmetry toward lower frequency side. The intense peak near 515 cm^{-1} and the asymmetric response at around 505 cm^{-1} correspond to atomic vibrations from Si crystalline core and near-surface regions, respectively [37]. Moreover, we did not observe any significant peaks related to Si–O bonds near 476 cm^{-1}. Hence, it is confirmed that the observed Raman spectra are dominated by the scattering of crystalline Si nanoparticles. The observed shift in Raman peak position is normally attributed to quantum confinement effects in Si NPs. Hence it can be connected with nanoparticle size (d) as per quantitative bond polarizability model [38, 39] by Eq. 1.

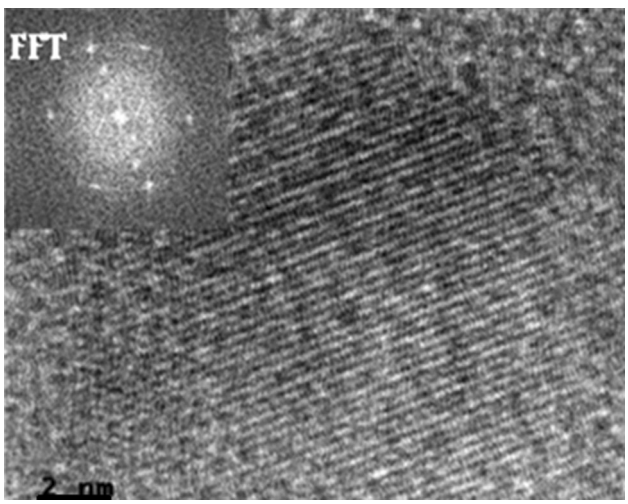

Fig. 5 The fast Fourier transform (*inset*) and inverse fast Fourier transform of a single Si NP obtained by HRTEM

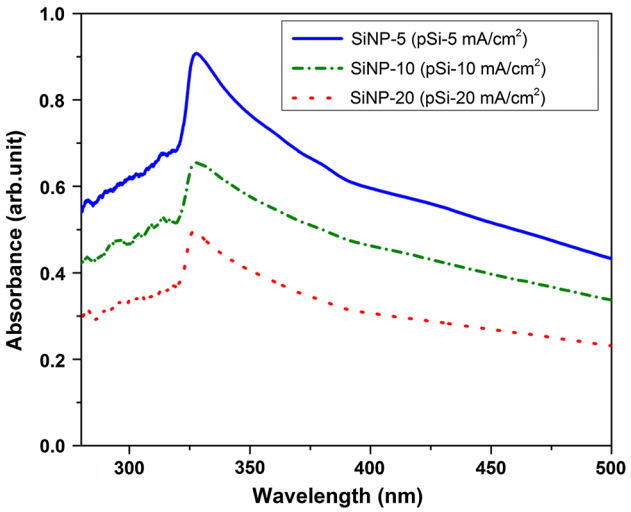

Fig. 6 UV–Vis absorption spectra of colloidal Si NPs generated with different pSi targets by laser ablation

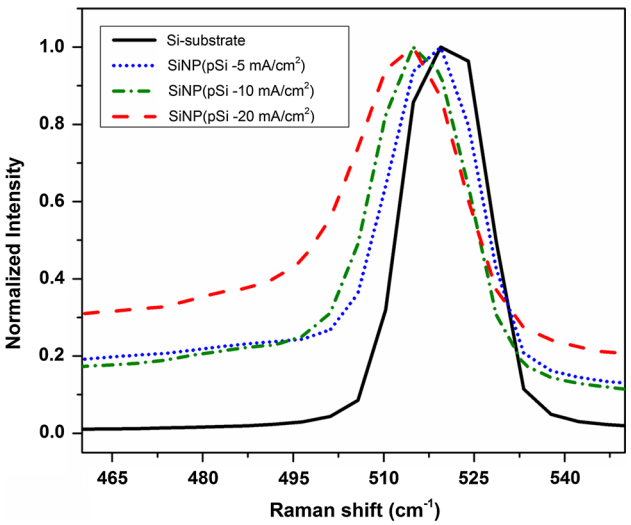

Fig. 7 Raman spectra of Si NPs synthesized by femtosecond laser ablation of pSi prepared at different etching current densities

$$\Delta v = -\alpha(0.543\ \text{nm}/d)^{\gamma}, \quad (1)$$

where Δv is the shift in the Raman peak position (Lorentz peak fitting has been used to find out the peak position) with respect to bulk Si value (520.4 cm^{-1}) and α (47.4 cm^{-1}), γ (1.44) are fitting constants. As shown in Table 2, the sizes of Si NPs as estimated by this technique are comparable to those obtained by TEM measurements.

Photoluminescence (PL) measurements have also been performed to study the emission properties of Si NPs. Figure 8 shows the PL spectra of Si NPs obtained by ablating pSi targets which were prepared at different etching current densities. The PL spectra were rather broad, ranging from 400 to 500 nm, with a maximum intensity at around 430 nm. The PL peak position was found to shift

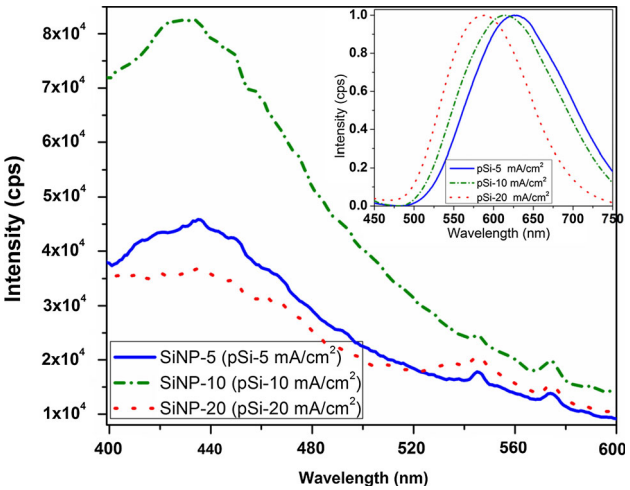

Fig. 8 Photoluminescence spectra of pSi before ablation (*inset*) and that of the colloidal Si NPs generated by laser ablation of porous silicon prepared at various etching current densities (Note: The concentration of Si NPs is expected to be different in different liquid samples. Hence the changes in intensity may not be interpreted in terms of physical parameters like size, etc.)

slightly toward the lower wavelengths as particle size decreased. This observation is also in agreement with quantum confinement effects [40]. Here it is important to mention that the expected shift in PL peak position for the kind of smaller size variations is generally less than the FWHM in case of pSi and Si NPs. Hence, it is not reasonable to estimate the particle size based on PL data. However, the observed small blue shifts still indicate the fact that there are more number of smaller Si NPs when compared to other samples. PL spectra obtained from pSi samples prepared at different etching current densities are shown in the inset of Fig. 8 (i.e., before ablation). As observed from Fig. 8, the most prominent difference between the PL data of Si NPs and pSi is that Si NPs give blue luminescence (see Table 2) whereas pSi gives red emission (see Table 1). It is well known that the pSi always gives bright orange to red emission although there are smaller nanoparticles in it [2]. Apparently, the blue luminescence is possible only when those smaller Si NPs are isolated from remaining Si network. Laser ablation was performed in the present work to separate these particles from bulk silicon and to prepare isolated, colloidal Si NPs. In addition, the generation of ultra-small Si NPs is expected because ablation may further break these smaller Si NPs when compared to the ablation of bulk Si. Therefore, our study suggests that the ablation of pSi produces smaller nanoparticles with small size distribution with less concentration of larger particles. Further the ablation process was found to depend on the initial porosity of silicon indicating the fact that the ablation of pSi is distinctly different from that of bulk silicon.

Conclusions

Ultra-small silicon nanoparticles were synthesized by ablating porous silicon using femtosecond laser in liquid medium. The size distribution of these silicon nanoparticles is estimated to be in the range of 1–10 nm by different techniques. HRTEM image of a single isolated Si NP shows the crystalline lattice fringes with lattice spacing of 0.31 nm corresponding to the inter-planar spacing of [111] planes in Si lattice. The crystalline structure of the generated silicon nanoparticles has been confirmed by SAED and Raman spectroscopy. The observed blue shift in absorption peak position with increase in etching current density is attributed to changes in average particle size. Similarly, the PL peak position was also found to shift toward lower wavelength regime. These results are in good agreement with quantum confinement effects. This study shows that the process of ablation depends on the initial porosity of pSi indicating the fact that the ablation of pSi is distinctly different from that of bulk silicon. Further, the ablation of porous silicon targets offers additional parameters for controlling the size and shape of nanoparticles produced.

Acknowledgement VSV thanks CSIR New Delhi for SRF in the Emeritus Scientist project awarded to APP. SVN and SVR thank UPE, UH for financial support in the form of a research project (UPE-II R-36, UH). SVR acknowledges continued financial support from DRDO.

References

1. Pavesi L, Turan R (2010) Silicon nanocrystals: fundamentals, synthesis and applications. Wiley, Germany
2. Vendamani VS, Nageswara Rao SVS, Pathak AP (2013) Structural and optical properties of porous silicon prepared by anodic etching of irradiated silicon. Nucl Instrum Method Phys B 315:188–191
3. Nageswara Rao SVS, Vendamani VS, Satrasala SK, Padhe SK, Srinadha Rao K, Dhamodaran S, Pathak AP (2011) Ion beam studies of semiconductor nanoparticles for the integration of optoelectronic devices. AIP Conf Proc 1336:332–336
4. Saikiran V, Vendamani VS, Hamad S, Nageswara Rao SVS, Venugopal Rao S, Pathak AP (2014) 150 MeV Au ion induced modification of Si nanoparticles prepared by laser ablation. Nucl Instrum Method Phys B 333:99–105
5. Mangaiyarkarasi D, Breese MBH, Ow YS, Vijila C (2006) Controlled blue shift of the resonant wavelength in porous silicon micro cavities using ion irradiation. Appl Phys Lett 89:021910-1–021910-3
6. Weiss SM, Haurylau M, Fauchet PM (2003) Tunable porous silicon mirrors for optoelectronic application. Mater Res Soc Symp Proc 737:529–534
7. Lek Ng W, Lourenco MA, Gwilliam RM, Ledain S, Shao G, Homewood KP (2001) An efficient room-temperature silicon-based light-emitting diode. Nature 410:192–194
8. Pavesi L, Dal Negro L, Mazzoleni C, FranzoA G, Priolo F (2000) Optical gain in silicon nanocrystals. Nature 408:440–444

9. Manilov AI, Skryshevsky VA (2013) Hydrogen in porous silicon: a review. Mater Sci Eng B 178:942–955
10. Blauwe JD (2002) Nanocrystal nonvolatile memory devices. IEEE Trans Nanotechnol 1:72–77
11. Rajabi M, Dariani RS (2009) Current improvement of porous silicon photovoltaic devices by using double layer porous silicon structure: applicable in porous silicon solar cells. J Porous Mater 16:513–519
12. Rogozhina E, Belomoin G, Smith A, Abuhassan L, Barry N, Akcakir O, Braun PV, Nayfeh MH (2001) Si–N linkage in ultra bright, ultrasmall Si nanoparticles. Appl Phys Lett 78:3711–3713
13. Belomoin G, Therrien J, Smith A, Rao S, Twesten R, Chaieb S, Nayfeh MH, Wagner L, Mitas L (2002) Observation of a magic discrete family of ultra bright Si nanoparticles. Appl Phys Lett 80:841–843
14. Canham LT (1990) Silicon quantum wire array fabrication by electrochemical and chemical dissolution of wafers. Appl Phys Lett 57:1046–1048
15. Zhou XD, Ren F, Xiao XH, Cai GX, Jiang CZ (2009) Influence of annealing temperatures and time on the photoluminescence properties of Si nanocrystals embedded in SiO_2. Nucl Instrum Method Phys Res B 267:3437–3442
16. Normand P, Kapetanakis E, Dimitrakis P, Tsoukalas D, Beltsios K, Cherkashin N, Bonafos C, Benassayag G, Coffin H, Claverie A, Soncini V, Agarwal A, Ameen M (2003) Effect of annealing environment on the memory properties of thin oxides with embedded Si nanocrystals obtained by low-energy ion-beam synthesis. Appl Phys Lett 83:168–170
17. Nakaso K, Han B, Ahn KH, Choi M, Okuyama K (2003) Synthesis of non-agglomerated nanoparticles by an electro spray assisted chemical vapor deposition (ES-CVD) method. J Aerosol Sci 34:869–872
18. Chicbkov BN, Momma C (1996) Femtosecond, picoseconds and nanosecond laser ablation of solids. Appl Phys A 63:109–115
19. Hamad S, Podagatlapalli GK, Vendamani VS, Nageswara Rao SVS, Pathak AP, Tewari SP, Venugopal Rao S (2014) Femtosecond ablation of silicon in acetone: tunable photoluminescence from generated nanoparticles and fabrication of surface nanostructures. J Phys Chem C 118:7139–7151
20. Gamaly EG (2011) The physics of ultra-short laser interaction with solids at non-relativistic intensities. Phys Rep 508:91–243
21. Tsuji T, Iryo K, Watanabe N, Tsuji M (2002) Preparation of silver nanoparticles by laser ablation in solution: influence of laser wavelength on particle size. App Surf Sci 202:80–85
22. Tsuji T, Kakita T, Tsuji M (2003) Preparation of nano-size particles of silver with femto second laser ablation in water. Appl Surf Sci 206:314–320
23. Shafeev GA, Freysz E, Bozon-Verduraz F (2004) Self-influence of a femtosecond laser beam upon ablation of Ag in liquids. Appl Phys A 78:307–309
24. Mafune F, Kohno J, Takeda Y, Kondow T, Sawabe H (2000) Formation and size control of silver nanoparticles by laser ablation in aqueous solution. J Phys Chem B 104:9111–9117
25. Yang G (2012) Laser ablation on liquids: principles and applications in the preparation of nanomaterials. Pan Stanford Publishing, Singapore
26. Podagatlapalli GK, Hamad S, Sreedhar S, Tewari SP, Venugopal Rao S (2012) Fabrication and characterization of aluminum nanostructures and nanoparticles obtained using femtosecond ablation technique. Chem Phy Lett 530:93–97
27. Hamad S, Podagatlapalli GK, Tewari SP, Venugopal Rao S (2013) Influence of picosecond multiple/single line ablation on copper nanoparticles fabricated for surface enhanced Raman spectroscopy and photonics applications. J Phys D 46:485501-1–485501-14
28. Rioux D, Laferrière M, Douplik A, Shah D, Lilge L, Kabashin AV, Meunier MM (2009) Silicon nanoparticles produced by femtosecond laser ablation in water as novel contamination-free photo sensitizers. J Biomed Opt 14:021010-1–021010-5
29. Blandin P, Maximova KA, Gongalsky MB, Sanchez-Royo JF, Chirvony VS, Sentis M, Timoshenko VY, Kabashin AV (2013) Femtosecond laser fragmentation from water-dispersed micro colloids: toward fast controllable growth of ultrapure Si-based nanomaterials for biological applications. J Mater Chem B 1:2489–2495
30. Abderrafi K, Calzada RG, Gongalsky MB, Suarez I, Abarques R, Chirvony VS, Timoshenko VY, Ibanez R, Martínez-Pastor JP (2011) Silicon nanocrystals produced by nanosecond laser ablation in an organic liquid. J Phys Chem C 115:5147–5151
31. Intartaglia R, Bagga K, Brandi F, Das G, Genovese A, Fabrizio ED, Diaspro A (2011) Optical properties of femtosecond laser-synthesized silicon nanoparticles in deionized water. J Phys Chem C 115:5102–5107
32. Semaltianos NG, Logothetidis S, Perrie W, Romani S, Potter RJ, Edwardson SP, French P, Sharp M, Dearden G, Watkins KG (2009) Silicon nanoparticles generated by femtosecond laser ablation in a liquid environment. J Nanopart Res 12:573–578
33. Chen L, Jiang XF, Guo Z, Zhu H, Kao TS, Xu QH, Ho GW, Hong M (2014) Tuning optical nonlinearity of laser-ablation-synthesized silicon nanoparticles via doping concentration. J Nanomater 2014:1–7
34. Alkis S, Okyay AK (2012) Post-treatment of silicon nanocrystals produced by ultra-short pulsed laser ablation in liquid: toward blue luminescent nanocrystals generation. J Phys Chem C 116:3432–3436
35. Tilaki RM, Irajizad A, Mahdavi SM (2006) Stability, size and optical properties of silver nanoparticles prepared by laser ablation in different carrier media. Appl Phys A 84:215–219
36. Han J, Li Y (2011) Interaction between pulsed laser and materials. In: Jakubczak K (ed) Lasers—applications in science and industry. InTech. http://www.intechopen.com/books/lasers-applications-in-science-and-industry/interaction-between-pulsed-laser-and-materials
37. Xia Hua, He YL, Wang LC, Zhang W, Liu XN, Zhang XK, Feng D (1995) Phonon mode study of Si nanocrystals using micro-Raman spectroscopy. J Appl Phys 78:6705–6708
38. Zi J, Zhang K, Xie X (1997) Comparison of models for Raman spectra of Si nanocrystals. Phys Rev B 55:9263–9266
39. Zi J, Buscher H, Falter C, Ludwig W, Zhang K, Xie X (1996) Raman shifts in Si nanocrystals. Appl Phys Lett 69:200–202
40. Barbagiovanni EG, Lockwood DJ (2012) Quantum confinement in Si and Ge nanostructures. J Appl Phys 111:034307-1–034307-9